JACS
JOURNAL OF THE AMERICAN CHEMICAL SOCIETY
Article
pubs.acs.org/JACS

Solvation Reaction Field at the Interface Measured by Vibrational Sum Frequency Generation Spectroscopy

Shayne A. Sorenson, Joel G. Patrow, and Jahan M. Dawlaty*

Department of Chemistry, University of Southern California, Los Angeles, California 90089, United States

Supporting Information

ABSTRACT: Interfacial electric fields are important in several areas of chemistry, materials sciences, and device physics. However, they are poorly understood, partly because they are difficult to measure directly and model accurately. We present both a spectroscopic experimental investigation and a theoretical model for the interfacial field at the junction of a conductor and a dielectric. First, we present vibrational sum frequency generation (VSFG) results of the nitrile (CN) stretch of 4-mercaptobenzonitrile (4-MBN) covalently attached to a gold surface and in contact with a variety of liquid dielectrics. It is found that the CN stretch frequency red-shifts with increasing dielectric constant. Second, we build a model in direct analogy to the well-known Onsager reaction field theory, which has been successful in predicting vibrational frequency shifts in bulk dielectric media. Clearly, due to the asymmetric environment, with metal on one side and a dielectric on the other, the bulk Onsager model is not applicable at the interface. To address this, we apply the Onsager model to the interface accounting for the asymmetry. The model successfully explains the red-shift of the CN stretch as a function of the dielectric constant and is used to estimate the reaction field near the interface. We show the similarities and differences between the conventional bulk Onsager model and the interfacial reaction field model. In particular, the model emphasizes the importance of the metal as part of the solvation environment of the tethered molecules. We anticipate that our work will be of fundamental value to understand the crucial and often elusive electric fields at interfaces.

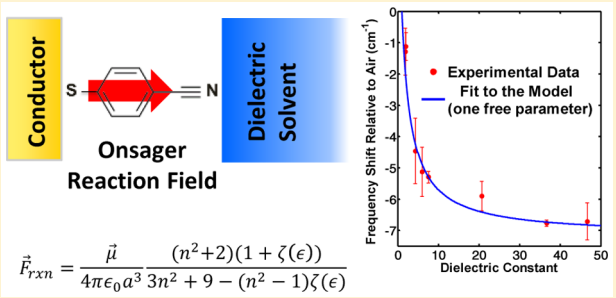

INTRODUCTION

Interfacial fields and energetics play a central role in several areas of contemporary physical sciences.[1−8] Two prime examples are photovoltaics and electrochemical interfaces, in which the central functions, charge separation and catalysis, are carried out at the interface. Despite the importance of interfacial phenomena, direct measurement of interfacial properties is often challenging. It is desirable to measure the local electric field near an interface directly. Previous attempts to measure interfacial electric fields have been made by spectroscopically monitoring the induced vibrational Stark shift of a probe chromophore at an interface.[9−13] These studies, for the most part, have focused on measuring the interfacial electric field due to an applied external potential. It is important to note, however, that local electric fields exist even in the absence of an applied external potential and critically influence the chemistry and physics of the interface. In this study, we investigate these type of inherent local electric fields.

The Stark shift of vibrational chromophores has been investigated in several contexts.[14−22] Boxer's group has pioneered the use of vibrational chomophores to study the local fields in confined biological environments such as proteins.[23−28] This approach relies on calibration of the frequency shift of the vibrational chromophore with respect to the electric field felt by the chromophore. This can be accomplished by two different methods. The first, and most relevant to this study, involves monitoring the change in a vibrational signature, like a CN stretch, in a variety of solvents that have no specific interactions, such as hydrogen bonding, with the solute as has been done in the bulk.[26,29] A simple description of this solvent-induced vibrational shift is based on the Stark effect and the well-known Onsager solvation theory.[30] According to this theory, the solute is modeled as residing in a spherical cavity and exerting a polarization on the surrounding solvent. The polarized solvent, in turn, creates a field in the cavity occupied by the solute, known as the Onsager reaction field. Thus, the vibrational frequency of the solute undergoes a Stark shift due to this field. Previous studies have successfully established a relationship between the local field strength and vibrational frequency shifts based on spectroscopic measurements in a variety of solvents.[31,32] The second calibration method is vibrational Stark spectroscopy, in which the influence of an externally applied electric field on a vibrational probe is studied.[25,33] Both of these methods have been shown to yield similar relationships between frequency and electric field. Once this relationship is established for a given chromophore, it can be used to infer the local field values by measuring the vibrational probe frequency when placed in an environment of interest such as a protein. This approach and its variants have

Received: November 18, 2016
Published: January 19, 2017

DOI: 10.1021/jacs.6b11940
J. Am. Chem. Soc. 2017, 139, 2369−2378

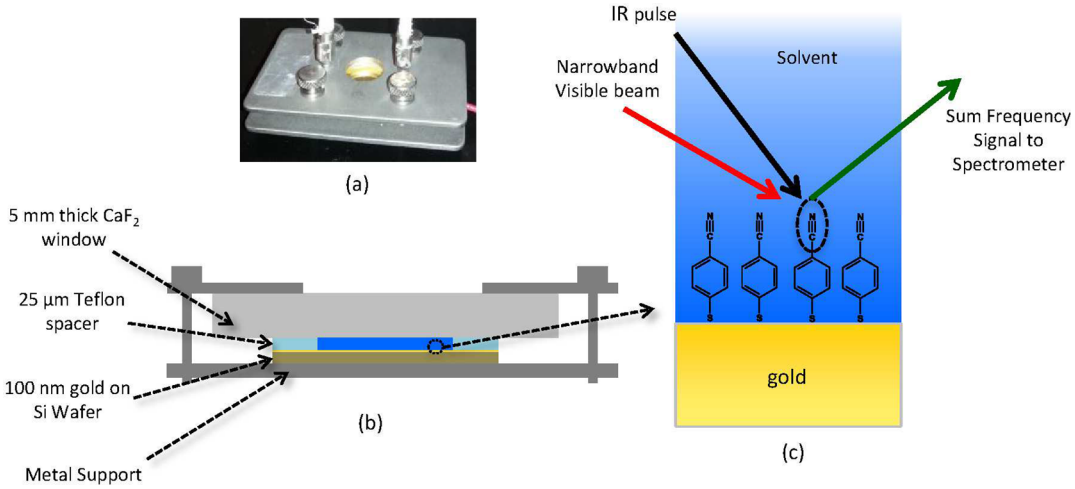

Figure 1. (a) A picture of the cell used in the experiments. (b) Diagram showing a cross section of the cell. (c) Cartoon diagram showing the incoming laser pulses and the outgoing sum frequency generation signal.

been used to estimate fields inside enzymes. Hammes-Schiffer and co-workers have undertaken theoretical work to understand the local fields measured using such methods.[27,28] Theoretical work by Cho and co-workers have underlined the potential of vibrational Stark probes in other contexts as well, such as hydrogen bond dynamics and structure.[16,18]

It is tempting to apply the bulk reaction field model to understand electric fields at the interface of a dielectric solvent and a conductor. However, one quickly realizes that several features of the Onsager model can not be directly translated to the interface. Setting aside the experimental difficulties of measuring the vibrational signal from the interface, one faces a more fundamental issue. The interface is inherently asymmetric in dielectric properties. A vibrational chromophore tethered to a metal surface and in contact with a dielectric senses a highly polarizable conductor on one side and a dielectric on the other. The reaction field induced by its image dipole in the metal and its polarization field in the dielectric is expected to be different from the Onsager field in the bulk. Therefore, the relationships mentioned before between the local field and vibrational frequency shifts need to be revisited for the interface. Our work aims to address this issue. We establish the basic relationship between vibrational frequency shift and the dielectric constant of a solvent when the vibrational chromophore resides in the asymmetric environment between a conductor and a dielectric. We propose that if the vibrational frequency shift in such an environment is understood well, it will pave the way for understanding more complicated scenarios such as measuring local fields near active electrochemical surfaces.

To measure the vibrational response of the interface, we use sum frequency generation, which is a well-established method of probing interfaces.[21,34−37] Then, in direct analogy to Onsager's reaction field for the bulk, we construct a model that describes the reaction field of the interfacial environment felt by the tethered molecule. We choose SFG spectroscopy for several reasons including its superior sensitivity to surface adsorbed species even at lower surface coverage and very small illumination areas, as well as its inherent surface selectivity and time-resolving capability, which we anticipate utilizing in future studies. We have measured the FTIR reflectance of 4-MBN on gold in contact with air (see Supporting Information) and observe the center wavelength of the CN stretch to be in excellent agreement with previously reported experiments[13] as well as our measured SFG spectra reported herein. We, therefore, believe that similar results to those presented here would be obtained by other methods such as IR reflection spectroscopy.

We point out that several previous works have used vibrational Stark shifts to measure local electric fields including their time-dependence in complicated environments. Vibrational Stark shifts have also been used to study the interfaces of photovoltaics.[5] Several works have reported the vibrational frequency shifts near an electrode surface.[9,10,13,21,38,39] Such measurements are of great value to practical electrochemistry problems in which the decay of an applied potential in the vicinity of the interface is important for redox chemistry. To achieve the important goals aspired by such studies, it is necessary to understand the baseline, which is the environment between a metal and a dielectric in the absence of an external field. Our work achieves this task.

Specific interactions with the solvent, such as hydrogen bonding, are known to interfere with the vibrational frequency of probes.[14,26,31,40−42] We also report solvents for which specific interactions with the nitrile probe, in particular hydrogen bonding and halogen bonding, result in deviations from a simple reaction field model. This aspect of our work is expected to guide future studies in which the vibrational probe is expected to be used in electrolyte−electrode interfaces where a large variety of interactions, including hydrogen bonding, can interfere with an unambiguous measurement of the local field.

This paper is arranged as follows. First, we describe our experiment and the results. Second, we provide a brief discussion of the Onsager model and then move on to create a reaction field model for the interface. Then, we calculate the Stark shift due to the reaction field on the vibrational chromophores and compare the results with the experiment. Finally, we discuss the shortcomings of the proposed model and suggest future theoretical and experimental work for its further improvement.

EXPERIMENTAL SECTION

Self-assembled monolayers (SAMs) of 4-mercaptobenzonitrile (4-MBN) were prepared on silicon wafers with a 10 nm Ti adhesion layer and 100 nm of Au purchased from LGA Thin Films, Inc. Wafers were cleaned by sonication in acetone twice, then in ethanol twice for 8 min each time, then immersed in a 0.03 M solution of 4-MBN in ethanol

DOI: 10.1021/jacs.6b11940
J. Am. Chem. Soc. 2017, 139, 2369−2378

for at least 24 h, which ensures full surface coverage for good signal quality.[21] After soaking in the 4-MBN solution, the wafers were removed and again sonicated twice in ethanol for 8 min each. Vibrational sum frequency generation (VSFG) spectra of these samples were taken in a demountable liquid FTIR cell (International Crystal Laboratories) modified for this purpose (see Figure 1). The back window of the cell was removed and replaced with the SAM containing wafer and a 25 μm Teflon spacer was placed directly on the sample surface. The front window of the demountable cell is a 4 mm thick CaF_2 window with small holes drilled to allow access to the cavity formed by the Teflon spacer between the wafer and the window. The entire assembly is then held firmly together using stainless steel plates and screws. Solvents were introduced by a syringe through the filling ports of the cell and reservoirs of solvent were subsequently attached to each port such that there was a constant supply to counter the losses due to evaporation or leaks during the experiment.

A 1 kHz regeneratively amplified Ti:Sapph laser (Coherent) was used to generate ultrafast near-IR pulses. A portion (1 W) of this was directed to an optical delay stage followed by a 4f filter to significantly narrow the spectrum, while another portion (2 W) was directed to an OPA (Coherent OPerA Solo) equipped with a $AgGaS_2$ crystal for difference frequency generation of mid-IR pulses. The 4f filter used two transmissive volume phase gratings (BaySpec, Inc.), two cylindrical lenses, and a variable width slit to filter the near-IR pulse to a spectral width of 8.0 cm^{-1}, centered at 787.62 nm. Typical spectra of both the near-IR upconversion pulses as well as the broadband mid-IR pulses can be found in the Supporting Information. Pulse energies were measured at the sample position to be 8.43 μJ for the near-IR and 7.56 μJ for the mid-IR. VSFG spectra were acquired by focusing these two pulses together on the sample using a common parabolic mirror and overlapping them in time. The angles of incidence relative to normal on the front face of the CaF_2 window were measured to be about 45° and 59° for the mid-IR and near-IR pulses, respectively. Using Snell's law and tabulated data for refractive indices,[43,44] the angles of incidence on the sample for the near-IR pulses are estimated to be between 29° and 33° for the range of dielectric solvents used. The range of incidence angles on the sample for the mid-IR pulses is expected to be centered around 37°; however refractive index data was not available for most solvents in the IR range of interest. Given the variation in the IR spectra of the solvents in the neighborhood of 2200 cm^{-1}, we expect the range in incidence angles for the mid-IR beam to be larger than that of the near-IR beam. The resulting SFG signal was collected with a second parabolic mirror and passed through a notch filter and a short pass filter to reject the majority of the scattered near-IR photons. All spectra were collected in the PPP polarization combination, corresponding to IR, visible, and SFG fields in that order.

The SFG signal was then sent to a spectrometer (Horiba iHR320) with a CCD camera (Princeton Instruments Pixis 300) for spectral analysis. With the input slit of the spectrometer set to 10 μm and using an 1800 gr/mm grating, the theoretically achievable spectral resolution was 0.05 nm (about 1 cm^{-1} in the spectral range of interest), which is well below the width of the near-IR upconversion pulse. In the traditional sense, the spectral resolution of the SFG spectra are, thus, limited by the 8 cm^{-1} width of the near-IR upconversion pulses. This is, by definition, the minimum wavenumber between two distinguishable peaks in the spectrum; however, for these experiments, we are only interested in the precision with which our spectroscopic system can determine the center frequency of a *single* peak. This is directly related to the resolution of the spectrometer, stated above to be closer to 1 cm^{-1}; thus our data reliably indicates peak shifts substantially smaller than the 8 cm^{-1} resolution. A single SFG spectrum is the result of a 100 s integration, and three such spectra were taken in succession. After this sequence of data collection, the cell was removed from the sample stage, inspected for bubbles in the cavity, then replaced on the sample stage, followed by another round of three spectra. This process was repeated three times for each solvent, resulting in a total of nine spectra for each solvent. Between solvents, the cell was flushed 10 times with 1 mL aliquots of the next solvent prior to filling the cell and collecting data.

DATA ANALYSIS

The VSFG spectrum of the benzonitrile tethered on gold necessarily has two components: the nonresonant signal from the gold and the resonant signal from the nitrile probe. Benderskii et al. have explained the interference of these two signals and proposed a model,[45] which we use in our experiment:

$$I_{SFG}(\omega) = \left| A_{NR}\, e^{i\phi} + \frac{B'}{\omega - \omega_{CN} + i\Gamma_{CN}} \right|^2 \exp\left(-\frac{(\omega - \omega_g)^2}{\sigma_g^{\,2}} \right) + C_{BG} \quad (1)$$

where the CN stretch vibration is characterized by its resonant frequency, ω_{CN}, width, Γ_{CN}, and *apparent* amplitude, B'. This model assumes a Gaussian IR pulse with center frequency, ω_g, width, σ_g^2, a constant nonresonant amplitude, A_{NR}, with a relative phase, ϕ. We measured a background spectrum by blocking the IR pulses and collecting a spectrum under otherwise identical conditions. This background spectrum was subtracted from each SFG spectrum; however, an additional term C_{BG} was still added to the model to account for an observed nonzero baseline likely caused by scattered light that was fairly constant across the spectrum and small compared to the SFG signal. Each of the nine spectra for each solvent were independently fit to this equation using Matlab's nonlinear least-squares fitting algorithm and the same initial guess. Figure 2a shows a representative spectrum with its fit. Figure 2b shows the Lorentzian components extracted from the fits. The average and standard deviation of each parameter for each solvent were then calculated using the nine fits. A table showing all of the fit parameters, their confidence intervals, and their standard deviations can be found in the Supporting Information.

RESULTS

The retrieved central frequencies from the above fitting procedure are shown in Figure 3. As a general trend, the frequency of the nitrile stretch red-shifts with increasing dielectric constant. In accordance with previous reports, hydrogen bonding solvents (water and methanol) clearly deviate from this trend. This phenomenon is very well understood and explained in detail in the literature.[14,26,31,40−42] In brief, it arises from hydrogen bonding to the lone pair of the CN group, which shifts the charge density away from the lone pair toward the hydrogen bond donor. The molecular orbital occupied by the lone pair has some CN antibonding character, and thus, when its electron density is reduced, the bond becomes stronger and the vibration blue-shifts overwhelming the red-shift expected from the dielectric constant. Furthermore, we observe the well-known halogen bonding effect on the CN stretch. Halogen bonding is a well-documented phenomenon[46,47] in which a halogen bearing group serves as an electron acceptor. The reason for this behavior is a region of reduced electronic charge density at the halogen end of the carbon−halogen bond known as a σ-hole. This σ-hole has been shown to serve as an electron acceptor and contributes to the formation of adducts[48] and stabilization of crystals[49] and influences surface reaction kinetics.[50] This effect may also be present in observed bulk Stark effect measurements.[26] In our case, the halogen σ-hole accepts electron density from the lone-pair of CN and induces a blue shift in the same way that was

DOI: 10.1021/jacs.6b11940
J. Am. Chem. Soc. 2017, 139, 2369−2378

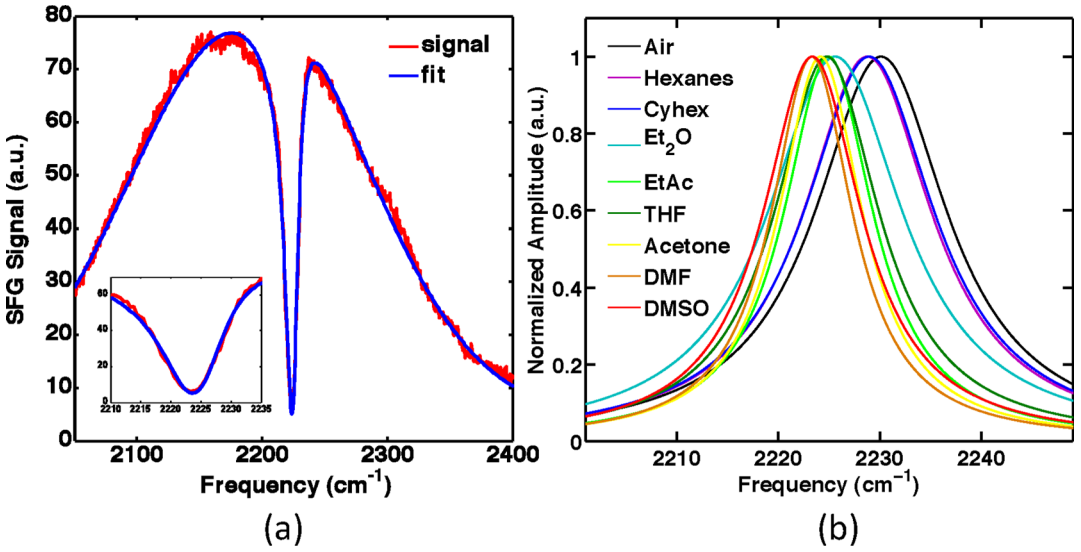

Figure 2. (a) A representative experimental raw signal shows a sharp line corresponding to the response of adsorbed nitrile superposed on a broad nonresonant signal. A fit based on interference of a Gaussian nonresonant background and a Lorentzian line shape for the nitrile stretch represents the data well. The inset shows a zoomed in portion of the spectrum near the nitrile stretch frequency. (b) Based on fits similar to the one shown in panel a, the spectrum of the nitrile stretch is isolated from the background. The data shows the variation of the spectrum when the surface is in contact with several solvents. Hydrogen-bonding and chlorinated solvents are omitted for clarity and shown in the SI.

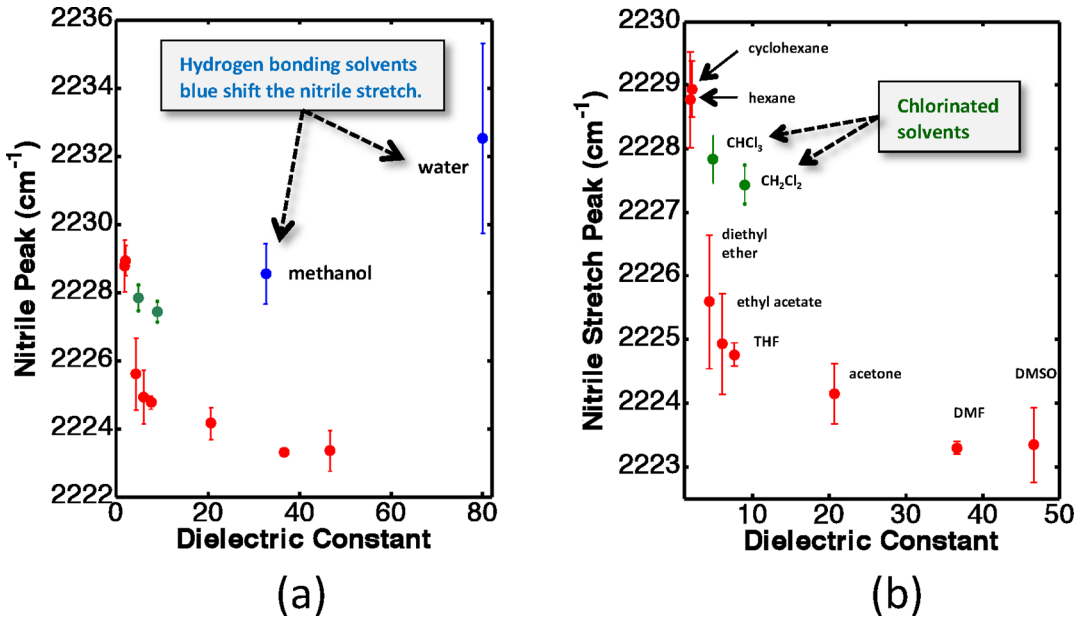

Figure 3. Observed frequency of the adsorbed nitrile stretch as a function of the dielectric constant of the solvent. (a) The hydrogen bonding solvents blue shift the stretch, consistent with a large body of previous observations in the bulk.[14,26,31,40−42] (b) Zoomed-in view of the data shown in panel a. The halogenated solvents show a clear deviation from a qualitative trend, which we hypothesize is due to halogen bonding. The model developed in the text explains the trend in the data.

just explained for the hydrogen bond. These two types of specific interactions, hydrogen bonding and halogen bonding, require further theoretical work and detailed computations. An electrostatic analysis, in the spirit of Onsager's model developed in the next section, cannot capture these effects. For that reason, we highlight the hydrogen-bonding and halogen-bonding data points with different colors and do not attempt to fit them to the new reaction field model.

THE REACTION FIELD MODEL FOR THE INTERFACE

The Bulk Onsager Model. Since our purpose is to modify the bulk Onsager reaction field theory for the metal−dielectric interface, it is necessary to briefly outline the structure of Onsager's approach[30] for easy identification of the components that need to be changed. A molecule with dipole moment, $\vec{\mu}$, and polarizability, α, when immersed in a dielectric continuum will polarize the surrounding medium. Onsager's critical insight was that the created polarization field in the dielectric will, in-turn, create a reaction field $\vec{F}_{rxn}$ at the site of the immersed

DOI: 10.1021/jacs.6b11940
J. Am. Chem. Soc. 2017, 139, 2369−2378

molecule. The molecule will respond to this reaction field proportional to its polarizability, α. Thus, at equilibrium, the molecule will have a dipole moment $\vec{m}$ that satisfies

$$\vec{m} = \vec{\mu} + \alpha\vec{F}_{rxn} \tag{2}$$

Consistent with intuition, the reaction field $\vec{F}_{rxn}$ is expected to be proportional to the dipole moment of the molecule

$$\vec{F}_{rxn,xn} = R\vec{m} \tag{3}$$

where R is a proportionality constant to be calculated from an electrostatics analysis as will be shown shortly. Substituting eq 3 into eq 2, one arrives at the value of the dipole moment when the molecule is immersed in the dielectric in terms of the unperturbed dipole moment, $\vec{\mu}$.

$$\vec{m} = \frac{\vec{\mu}}{1 - \alpha R} \tag{4}$$

The reaction field in eq 3, therefore, can be written in terms of the unperturbed dipole moment as follows:

$$\vec{F}_{rxn,xn} = \left(\frac{R}{1 - \alpha R}\right)\vec{\mu} \tag{5}$$

The next task is to write R and α in terms of experimentally measurable quantities. First, to relate R to the bulk dielectric constant, Onsager considered the molecule to reside in a spherical cavity of radius, a, carved in the dielectric medium. The potential inside the sphere was assumed to arise from the immersed dipole and the polarized dielectric in the surrounding (Figure 4b). The potential outside was assumed to be that of the immersed dipole modified by the dielectric. After applying the standard electrostatic boundary conditions, the value of R is found to be

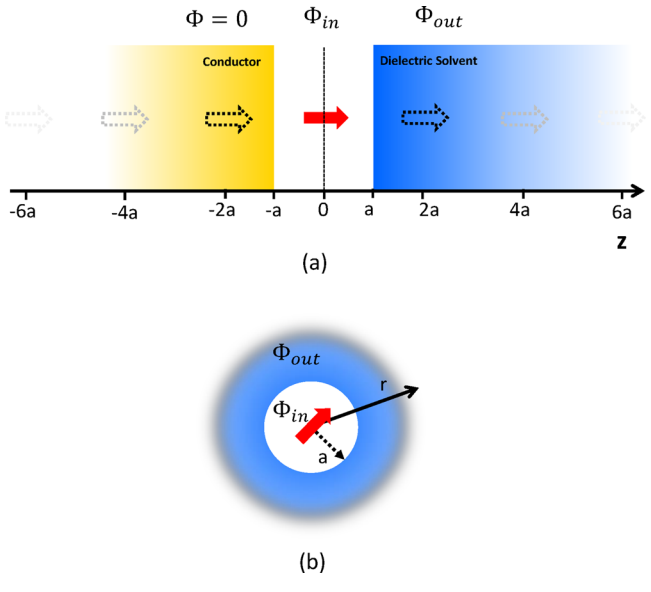

Figure 4. (a) A model that describes the interaction of a dipole with a conducting surface and an adjacent dielectric. In analogy to the Onsager model, the dipole resides in a cavity in the intervening space between the metal and the dielectric. The purpose of the model is to find the field inside this cavity, which arises due to the induced image dipoles in the metal (dashed arrows) and the dielectric. (b) The classic Onsager model showing a dipole residing in a cavity inside a dielectric medium is shown for contrast.

$$R = \frac{1}{4\pi\epsilon_o a^3}\frac{2(\epsilon_r - 1)}{2\epsilon_r + 1} \tag{6}$$

A relationship between the molecular polarizability, α, and the bulk refractive index, n, is already known under the name of the Lorentz–Lorenz equation:

$$\alpha = 4\pi\epsilon_o a^3\left(\frac{n^2 - 1}{n^2 + 2}\right) \tag{7}$$

Inserting eqs 6 and 7 into eq 5, one arrives at the final expression for the Onsager reaction field in terms of the dielectric constant of the surrounding medium and the refractive index of the immersed molecule.

$$\vec{F}_{rxn} = \frac{\vec{\mu}}{4\pi\epsilon_o a^3}\frac{2(\epsilon_r - 1)(n^2 + 2)}{3(n^2 + 2\epsilon_r)} \tag{8}$$

The power of eq 8 is that it relates a microscopic field felt by the solute molecules to the bulk dielectric constant of the surrounding, ϵ_r, and the bulk refractive index of the molecule, n. This relation has been used extensively by Boxer and others to analyze vibrational solvatochromism and to calibrate vibrational Stark shifts.[26,31,40,51−53] While more sophisticated approaches may be followed for increasingly precise calculations of the reaction field, the above expression still retains its power due to its simplicity and generality.

The Onsager Model for the Metal–Dielectric Interface. Because of the asymmetry, solvation at an interface is markedly different compared to solvation in the bulk. In the case of an interface composed of a metal and a dielectric solvent, both sides are involved in solvation. Using an approach similar to the Onsager model, we calculate the reaction field that a molecule experiences when placed at the junction of a metal and a dielectric. To distinguish it from the bulk case, we will identify it with a superscript $\vec{F}^{int}_{rxn}$. In direct analogy to the Onsager cavity, we envisage a planar cavity of thickness $2a$ separating the metal and the dielectric with dielectric constant, ϵ_r (Figure 4a). Then, we place a molecular dipole, oriented perpendicular to the metal, in the middle of the cavity. Due to the cylindrical symmetry of the system, we choose cylindrical coordinates $\{z, \rho\}$, with the dipole placed at $\{z = 0, \rho = 0\}$.

The dipole is expected to polarize both the dielectric and the metal, and these resulting polarizations will create a reaction field at the location of the dipole. Thus, the essence of eqs 2−5 will still hold. However, unlike the bulk case, the dipole feels an asymmetric environment, and consequently, the expected reaction field will be different from the bulk. Our goal is to find that field in direct analogy to Onsager's theory. The first step is to solve the electrostatic problem considering the appropriate boundary conditions for the two sides of the cavity.

The method of images, used often in elementary electrostatics, is a convenient and simple way to formulate the potential that satisfies both Laplace's equation and the problem-specific boundary conditions at conductor or dielectric interfaces. Given an idealized dipole at $z = 0$ above a conductor whose boundary is at $z = -a$, the potential arising from the induced polarization in the conductor measured on the free space side can be written as if arising from an image dipole at $z = -2a$. A dipole above a dielectric continuum similarly gives rise to a polarization potential that can be described by an image dipole, modified in this case by a constant that depends on ϵ_r. In this problem, we have two opposing interfaces with boundaries at $z = a$ and $z = -a$, and any image dipole in the

DOI: 10.1021/jacs.6b11940
J. Am. Chem. Soc. 2017, 139, 2369−2378

conductor (dielectric) will have its own image in the dielectric (conductor), giving way to an infinite array of image dipoles in both the conductor and the dielectric spaced at intervals of length $2a$ and modified by some coefficients yet to be determined (see Figure 4). It must be remembered that these images have no physical bearing. They simply serve as a basis set that satisfies Laplace's equation and adequately represents the apparently complicated polarization within the conductor and dielectric such that the boundary conditions are satisfied. The field within the cavity between the two interfaces due to these material polarizations can easily be obtained from the potential once the coefficients have been determined. The potential, as well as the z-component of the electric field due to a dipole located at $z = 2ja$, where j is an index of location, is given as

$$\phi_j(z, \rho) = \frac{|\vec{m}|}{4\pi\epsilon_o} \frac{z - 2ja}{(\rho^2 + (z - 2ja)^2)^{3/2}} \tag{9}$$

$$\vec{F}_{z,j}(z, \rho) = \frac{|\vec{m}|}{4\pi\epsilon_o} \frac{2(z - 2ja)^2 - \rho^2}{(\rho^2 + (z - 2ja)^2)^{5/2}} \hat{z} \tag{10}$$

Using the above expressions in combination with the geometry illustrated in Figure 4, the real dipole in the cavity corresponds to $j = 0$ and when $j < 0$ ($j > 0$), the dipole is in the conductor (dielectric). The total potential in the cavity can now be constructed as

$$\Phi_{in}(z, \rho) = \phi_0 + \sum_{j=-\infty}^{\infty} \mathcal{A}_j \phi_j \tag{11}$$

where $\mathcal{A}_j$ are the coefficients to be determined from enforcing the boundary conditions. The potential *in the dielectric* can be written as the sum of the potential due to the dipole and all of the images in the metal, attenuated by some constant in exact parallel to the single dielectric interface problem discussed above.

$$\Phi_{out}(z, \rho) = \mathcal{B}(\phi_0 + \sum_{j=-\infty}^{-1} C_j \phi_j) \tag{12}$$

The coefficients $\mathcal{A}_j$, $\mathcal{B}$, and C_j can be obtained by imposing the standard electrostatic boundary conditions with the metal held at zero potential:

$$\Phi_{in}(-a, \rho) = 0 \tag{13}$$

$$\Phi_{in}(a, \rho) = \Phi_{out}(a, \rho) \tag{14}$$

$$\left.\frac{\partial \Phi_{in}}{\partial z}\right|_a = \epsilon_r \left.\frac{\partial \Phi_{out}}{\partial z}\right|_a \tag{15}$$

We can find one form of the solution whose form is relatively simple by building up two images at a time and satisfying alternating boundary conditions. This procedure is explained fully in the Supporting Information; here we just give the full solution:

$$\Phi_{in} = \Phi_0 + \Phi_{-1} + \sum_{j=1}^{\infty} A^j(\Phi_{-2j} + \Phi_{-2j-1} + \Phi_{2j} + \Phi_{2j-1}) \tag{16}$$

$$\Phi_{out} = B(\Phi_0 + \Phi_{-1} + \sum_{j=1}^{\infty} A^j[\Phi_{-2j} + \Phi_{-2j-1}]) \tag{17}$$

where

$$A = \frac{\epsilon_r - 1}{\epsilon_r + 1} \quad \text{and} \quad \mathcal{B} = \frac{2}{\epsilon_r + 1} \tag{18}$$

The potential profile and the associated electric field (using eq 10) can now be evaluated to an arbitrary order of precision inside the cavity and in the dielectric. A representative picture of the potential profile and electric field lines is shown in the Supporting Information. Since we will be interested in the reaction field at the location of the dipole, $\{z = 0, \rho = 0\}$, we evaluate the electric field inside the cavity at this point, neglecting the contribution of the dipole in the cavity itself:

$$\vec{F}_{rxn}^{int} = R_{int}\vec{m} \equiv \frac{1}{16\pi\epsilon_o} \frac{\vec{m}}{a^3}(1 + \zeta(\epsilon)) \tag{19}$$

where

$$\zeta(\epsilon) \equiv \sum_j A^j \left(\frac{128j^6 + 12j^2 - 1}{4j^3(4j^2 - 1)^3} \right) \tag{20}$$

Though the infinite sum appears fairly complicated, it converges rapidly and only the first two or three terms make a significant contribution. A more detailed analysis of this sum and its convergence can be found in the Supporting Information.

Notice that, as expected, when $\epsilon_r = 1$, the reaction field is drastically simplified, taking a nonzero value of $\vec{F}_{rxn} = \vec{m}/(16\pi\epsilon_o a^3)$. Thus, unlike the bulk, a reaction field due to the image dipole in the metal will exist even when the adjacent medium is vacuum. Otherwise stated, the metal is a part of the solvation environment of the dipole and will respond and react to the dipole even in the absence of the dielectric.

The result for the reaction field shown in eq 19 is analogous to eq 3 and can be cast in the form of eq 5 in order to relate the reaction field to the unperturbed molecular dipole, $\vec{\mu}$, and molecular polarizability, α. As before, we will take α from the Lorentz–Lorenz relation (eq 7), such that the reaction field can be written as

$$\vec{F}_{rxn}^{int} = \frac{\vec{\mu}}{4\pi\epsilon_o a^3} \frac{(n^2 + 2)(1 + \zeta(\epsilon))}{3n^2 + 9 - (n^2 - 1)\zeta(\epsilon)} \tag{21}$$

This is the final equation for the reaction field of a perpendicular dipole at the interface of a dielectric and a metal in direct analogy to Onsager's bulk result in eq 8. The model can be easily modified to allow for dipoles at the surface that are tilted relative to the surface normal. We have derived an expression similar to eq 21 as a function of orientation angle in the Supporting Information. Assuming perpendicular orientation, the overall dependence of the field in eq 21 on ϵ_r is very similar to the Onsager model (as shown in Figure 5). However, unlike the bulk Onsager field, which (not surprisingly) vanishes for $\epsilon_r = 1$, the interfacial reaction field has a nonzero value, due to the interaction with the metal, as described before. Furthermore, the overall magnitude of $\vec{F}_{rxn}^{int}$ is smaller than its bulk counterpart for most dielectric constants. This is a distinguishing feature between the bulk and interfacial models and its consequences will be discussed later.

DOI: 10.1021/jacs.6b11940
J. Am. Chem. Soc. 2017, 139, 2369–2378

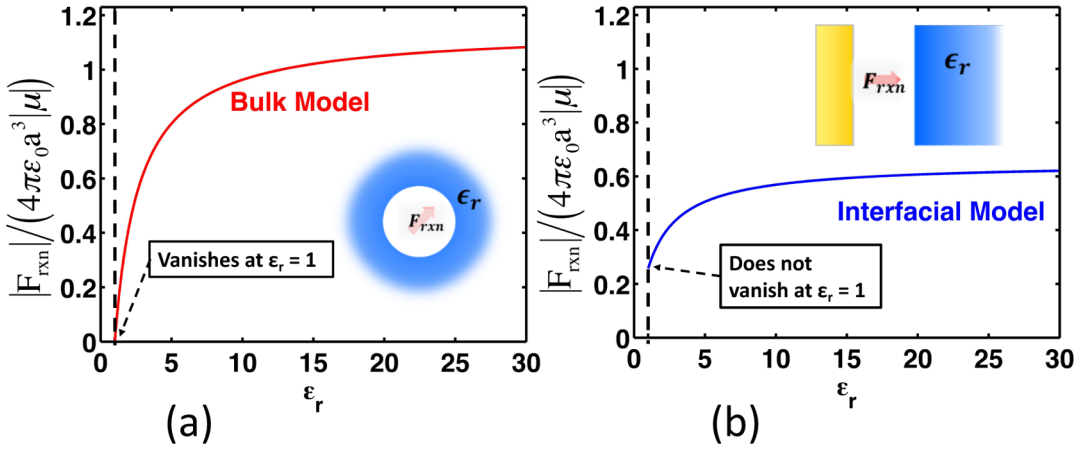

Figure 5. (a) The bulk Onsager reaction field (in reduced units) as a function of the dielectric constant of the surrounding. As expected for $\epsilon_r = 1$, the reaction field vanishes. (b) The interfacial reaction field, calculated based on eq 21. Unlike the bulk case, for $\epsilon_r = 1$, the reaction field is nonzero due to interaction with the metal.

Vibrational Stark Shift Due to the Reaction Field. Based on first order perturbation theory, the vibrational Stark shift $\Delta\nu = (E_1 - E_0)/h$ or the change in the vibrational spectroscopic gap is expressed as

$$h\Delta\nu = -\Delta\mu F \tag{22}$$

The factor $\Delta\mu = \mu_1 - \mu_0$ is the difference between dipole moments of the ground and excited vibrational states, and F is either an externally applied field or a local field felt by the molecule. The value of $\Delta\mu$ is a molecular property and within this level of perturbation remains independent of F. Therefore, $\Delta\mu$ is also known as the Stark tuning rate, which linearly relates the spectroscopic gap, $h\Delta\nu$, to the field, F.

In our experiments, the observable is $h\Delta\nu$ near the interface, which is the product of two unknowns: $\Delta\mu$ and the interfacial reaction field, $\vec{F}^{\text{int}}_{\text{rxn}}$. In the experiments reported here, we could not vary $\vec{F}^{\text{int}}_{\text{rxn}}$ other than by choice of solvent. As mentioned in previous sections, we do have a scaling relationship between the reaction field, $\vec{F}^{\text{int}}_{\text{rxn}}$, and the solvent, ϵ_r, in eq 21. We can, therefore, test the proposed model against the experimental results to see if the experimental frequency shifts exhibit the same ϵ_r dependence that is expected from the model. To achieve this, it is best to consider the frequency shift relative to a reference value. For the bulk model, the reference value is taken to be the vibrational frequency in vacuum ($\epsilon_r = 1$), which is 2242 cm^{-1}.[54] Here, we take the frequency shift $\Delta\nu$ to be relative to the experimentally measured frequency of 4-MBN tethered on gold when in contact with air ($\epsilon \approx 1$), which is $\nu(1) = 2230\ \text{cm}^{-1}$ measured by us and others.[13] Thus, the frequency shift is given by

$$h\Delta\nu(\epsilon_r) = h(\nu(\epsilon_r) - \nu(1)) = -\Delta\mu(\vec{F}^{\text{int}}_{\text{rxn}}(\epsilon_r) - \vec{F}^{\text{int}}_{\text{rxn}}(1)) \tag{23}$$

where $\vec{F}^{\text{int}}_{\text{rxn}}(\epsilon_r)$ is taken from eq 21. Note, however, that $\Delta\mu$ cannot be determined directly as a fitting parameter. The reaction field of eq 21 has the prefactor $\vec{\mu}/(4\pi\epsilon_o a^3)$, which multiplies $\Delta\mu$. Thus, what can be achieved from the experimental fit is not retrieval of $\Delta\mu$ but rather its product with the above prefactor. More explicitly, the above equation can be written as

$$h\Delta\nu(\epsilon_r) = \left(\frac{\vec{\mu}\,\Delta\mu}{4\pi\epsilon_o a^3}\right)\left(\frac{4(n^2+2)^2\zeta(\epsilon)}{3(n^2+3)[(n^2-1)\zeta(\epsilon) - 3n^2 - 9]}\right) \tag{24}$$

Once again, the dependence of the above expression on ϵ_r (the dielectric constant of the solvent) and n (the refractive index of the dipole bearing layer) is relatively simple. The relationship shows a monotonic red-shift of the vibrational frequency with respect to the dielectric constant. Equation 24 can be used to fit the experimental data to the model, with the prefactor being the *only* fitting parameter, and using the accepted value of $n = 1.528$ for benzonitrile. The result is shown in Figure 6. The prefactor is recovered from the least-squares fit as 15.0 cm^{-1} with an error of $\pm 1.3\ \text{cm}^{-1}$ at 95% confidence. The fit (blue line) in the figure captures the red-shift of the vibrational frequency with increasing dielectric constant reasonably well. Fit in hand, we are now equipped to state that hydrogen bonding with water apparently causes the CN stretch to shift by about 10 cm^{-1}, which is entirely

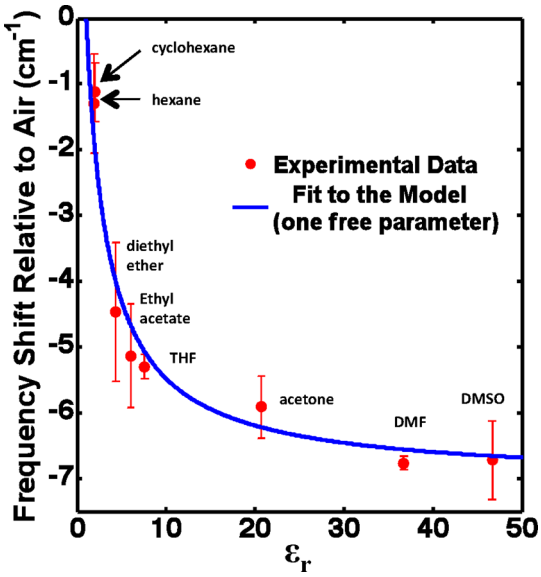

Figure 6. Experimental frequency shifts (red) and a single parameter fit to the model (blue). The *only* fitting parameter is the prefactor in eq 24, for which a value of 15.0 cm^{-1} is retrieved.

DOI: 10.1021/jacs.6b11940
J. Am. Chem. Soc. 2017, 139, 2369−2378

consistent with previous measurements.[53] We understand that such assignments must be approached with caution considering that the nonspecific and specific effects may not be merely additive and likely require considerations beyond an electrostatic model. Our data, however, appear to suggest a trend in the strengths of specific interactions with surface attached 4-MBN in the following order: H_2O > MeOH > CH_2Cl_2 > $CHCl_3$.

Now, we return to Figure 5, where a clear difference in the bulk and interfacial models is predicted. The span of reaction field values (range of $|F_{rxn}|$ from $\epsilon_r = 1$ to large values of ϵ_r) in the bulk is much larger than at the interface. Therefore, the Stark shift in the bulk relative to the gas phase (2242 cm^{-1})[54] is predicted to be larger than the interfacial Stark shift relative to the gold−air interface. This is consistent with our interfacial experiments and previous experiments in the bulk by Boxer et al. In our experiment, the largest shift, with respect to air, is about 7 cm^{-1}. Data in the bulk show a shift nearly double that amount (about 14.43 cm^{-1})[26] relative to the gas phase.

With the value of the prefactor in eq 24 determined experimentally, we will evaluate whether this number matches with expectations based on previous experimental and theoretical literature on benzonitriles. The three components of the prefactor are the adsorbed molecule's permanent dipole moment, μ, its change in dipole moment between the first excited vibrational state and the ground vibrational state, $\Delta\mu$, and the effective size of the cavity, $2a$. As a first estimate, we take the dipole value for benzonitrile from the established literature as μ = 4.48 D (Debye).[55] This value in combination with a reasonable theoretical value for the cavity width would allow us, in turn, to estimate the Stark tuning rate ($\Delta\mu$) of 4-MBN on gold. We estimate the cavity thickness as equal to the sulfur to nitrogen distance for 4-MBN of 7.15 Å (calculated using DFT at the B97XD level as implemented in Q-Chem). According to the proposed model, and using the prefactor from the experimental fit, this would correspond to a Stark tuning rate of $\Delta\mu$ = 0.030 D. Finally, if we assume the above values, we can estimate the value of the reaction field at the interface by using eq 21. As shown in Figure 7, the reaction field at the interface of the solvent and metal ranges from 9.80 MV/cm for hexane to 20.9 MV/cm for DMSO. The magnitudes of these field are within the expectations for reaction fields from solvents as reported previously.[26,51]

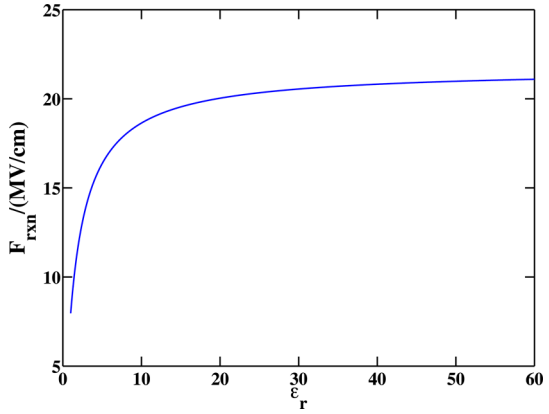

Figure 7. Value of reaction field at the metal−dielectric interface calculated based on the experimental data and the values of μ and $\Delta\mu$ for benzonitrile from previous work.

We point out that the values for μ and the cavity thickness that we have used in arriving at Figure 7 are somewhat speculative due to lack of data on adsorption geometry and possible change in μ because of the substituent and adsorption effects. Boxer et. al have measured the Stark tuning rate of benzonitrile to be between 0.012 and 0.018 D.[26,31,33] Though our estimate is on the same order, the agreement is not perfect, which shows that there is room for error in the value chosen for cavity thickness. It is also important to note that this discrepancy in Stark tuning rates is likely due, at least in part, to the fact that μ and $\Delta\mu$ vary with the Hammett parameter of a molecule's substituents.[33] To our knowledge, no systematic study of the Hammett parameter due to interaction with gold is known. Work on this front is currently underway by us and is the subject of future reports. However, it is worth noting that based on thiol's small Hammett parameter (σ_p = 0.15),[56] the Stark tuning rate of 4-MBN alone is expected to be close to that of benzonitrile.

CONCLUSION AND THE NEED FOR FUTURE WORK

Just like the bulk Onsager reaction field theory, the strength of the model developed above is its simplicity. A major finding from the model is that a reaction field near a conductor−dielectric interface can be calculated from a simple electrostatic analysis and the dependence of such a reaction field on the adjacent dielectric can be modeled via a simple relation. Not surprisingly, this simplicity and elegance comes at the cost of a few shortcomings. Some of these shortcomings are shared with the Onsager model, while some are unique to the interfacial problem. First, just as in the Onsager model, specific interactions such as hydrogen bonding and halogen bonding cannot be accounted for. This is evident in the deviation of the frequency shift from the expected dielectric behavior for the hydrogen bonding and halogen bonding solvents shown in Figure 3. Second, just as in the Onsager model, an accurate assignment of the cavity size is not evidently clear. While the cavity size may be roughly estimated from the length of a molecule, the inverse cube dependence makes the reaction field a sensitive function of the cavity size.

There are approximations and assumptions that are unique to the interfacial problem. First is the estimate of the polarizability, α, when writing eq 21. We have used the Lorentz−Lorenz equation (eq 7), which relates molecular polarizability to the bulk refractive index. Molecular polarizability is a tensor quantity. For our case of an array of aligned molecules near the interface, the most relevant value of the polarizability tensor is the polarizability along the CN axis or α_{zz}. We do not have direct access to this number, at least from this experiment; however an experimentally measured value has been reported for benzonitrile in the literature.[57] The value we obtain from the Lorentz−Lorenz equation agrees, within a factor of 2, with that reported by LeFevre et. al, which is less than the difference between the parallel and transverse polarizabilities in their study. Given the slight disparity with experiment and considering the lack of modern measurements, we hope that theoretical and computational results can address this quantity in the future. The next issue is the correction for local field due to interactions between the neighboring adsorbed molecules. Such an interaction may affect both the effective dielectric constant of the cavity (to a value different from ϵ_0) and the molecular polarizability, α. Determination of the local field correction due to intermolecular interactions within the layer is the subject of future work.

DOI: 10.1021/jacs.6b11940
J. Am. Chem. Soc. 2017, 139, 2369−2378

Another challenge that is unique to the interfacial problem is that of orientation of the dipole relative to the interface. Lacking a good experimental consensus on the orientation of the 4-MBN/Au system, the treatment above assumed a perpendicular orientation for the sake of simplicity. In our lab, we have taken polarization dependent FTIR reflectance measurements (shown in the Supporting Information) and see the complete disappearance of the CN stretch when the incident radiation is polarized parallel to the surface. This is consistent with a perpendicular orientation of the 4-MBN molecules on gold; however, we recognize that it may not be conclusive and more experiments are needed to verify this assumption. A few orientation angles have been offered for this system[13] or the similar thiophenol/Au system;[58,59] however the most direct experiments were unable to conclude whether thiophenol was tilted 49° from the surface normal or just randomly orientated. Furthermore, we have no indication of whether this orientation distribution will change when exposed to different solvent environments. Determination of the orientation angles of surface attached molecules is, in principle, obtainable by polarization dependent SFG studies. Such measurements on this system will be the subject of future measurements in our lab. We emphasize again that the model presented above relating the interfacial reaction field to the dielectric constant of the solvent can easily be extended to have dependence on the orientation angle of the dipole, as shown in the Supporting Information. A better experimental understanding of the orientation distribution in this system may ultimately lead to slight modification of the values for the interfacial field discussed above and given in Figure 7; however, any changes are expected to be at most about 10% (See Supporting Information).

We believe that theoretical and computational input can provide help in arriving at a more complete picture of interfacial fields, in particular by explicitly accounting for specific interactions (hydrogen and halogen bonding), local field effects due to intermolecular interactions, and explicit calculation of the relevant polarizability tensor elements. We also believe that the model and field values discussed here could serve as a launching point for the theoretical chemistry community in implementing implicit interfacial solvation models.

■ ASSOCIATED CONTENT

Supporting Information

The Supporting Information has This material is available free of charge via the Internet at http://pubs.acs.org/. The Supporting Information is available free of charge on the ACS Publications website at DOI: 10.1021/jacs.6b11940.

Spectra of the mid-IR and near-IR upconversion pulses, the polarization dependent FTIR reflectance data, plots of the raw data for each solvent, table showing the fit parameters for each solvent, and more detailed derivation of the interfacial reaction field, including its dependence on orientation angle (PDF)

■ AUTHOR INFORMATION

Corresponding Author

*dawlaty@usc.edu

ORCID

Jahan M. Dawlaty: 0000-0001-5218-847X

Notes

The authors declare no competing financial interest.

■ ACKNOWLEDGMENTS

The authors gratefully acknowledge support from the NSF CAREER Award (1454467), AFOSR YIP Award (FA9550-13-1-0128), The Rose Hills Foundation Award, and the Cottrell Scholar Award from the Research Corporation for Science Advancement.

■ REFERENCES

(1) Ardo, S.; Sun, Y.; Staniszewski, A.; Castellano, F. N.; Meyer, G. J. *J. Am. Chem. Soc.* **2010**, *132*, 6696.
(2) Chung, M. S.; Mayer, A.; Miskovsky, N. M.; Weiss, B. L.; Cutler, P. H. *Ultramicroscopy* **2013**, *132*, 41.
(3) Murgida, D. H.; Hildebrandt, P. *J. Phys. Chem. B* **2001**, *105*, 1578.
(4) Murgida, D. H.; Hildebrandt, P. *Acc. Chem. Res.* **2004**, *37*, 854.
(5) Pensack, R. D.; Asbury, J. B. *J. Am. Chem. Soc.* **2009**, *131*, 15986.
(6) Vanbel, M. K.; Su, C. Y.; Locquet, J. P.; Verbiest, T. *J. Phys. Chem. C* **2014**, *118*, 1919.
(7) Braun, S.; Salaneck, W. R.; Fahlman, M. *Adv. Mater.* **2009**, *21*, 1450.
(8) Makov, G.; Nitzan, A. *J. Phys. Chem.* **1994**, *98*, 3459.
(9) Oklejas, V.; Sjostrom, C.; Harris, J. M. *J. Am. Chem. Soc.* **2002**, *124*, 2408.
(10) Oklejas, V.; Harris, J. M. *Langmuir* **2003**, *19*, 5794.
(11) Siebert-Henze, E.; Lyssenko, V. G.; Fischer, J.; Tietze, M.; Brueckner, R.; Schwarze, M.; Vandewal, K.; Ray, D.; Riede, M.; Leo, K. *AIP Adv.* **2014**, *4*, 047134.
(12) Siebert-Henze, E.; Lyssenko, V. G.; Brückner, R.; Riede, M.; Leo, K. *MRS Online Proc. Libr.* **2014**, DOI: 10.1557/opl.2014.50.
(13) Schkolnik, G.; Salewski, J.; Millo, D.; Zebger, I.; Franzen, S.; Hildebrandt, P. *Int. J. Mol. Sci.* **2012**, *13*, 7466.
(14) Aschaffenburg, D. J.; Moog, R. S. *J. Phys. Chem. B* **2009**, *113*, 12736.
(15) Boxer, S. G. *J. Phys. Chem. B* **2009**, *113*, 2972.
(16) Choi, J. H.; Cho, M. *J. Chem. Phys.* **2011**, *134*, 154513.
(17) Nydegger, M. W.; Dutta, S.; Cheatum, C. M. *J. Chem. Phys.* **2010**, *133*, 134506.
(18) Maj, M.; Ahn, C.; Błasiak, B.; Kwak, K.; Han, H.; Cho, M. *J. Phys. Chem. B* **2016**, *120*, 10167.
(19) Koch, M.; Licari, G.; Vauthey, E. *J. Phys. Chem. B* **2015**, *119*, 11846.
(20) Stamenkovic, V.; Chou, K. C.; Somorjai, G. A.; Ross, P. N.; Markovic, N. M. *J. Phys. Chem. B* **2005**, *109*, 678.
(21) Humbert, C.; Busson, B.; Six, C.; Gayral, A.; Gruselle, M.; Villain, F.; Tadjeddine, A. *J. Electroanal. Chem.* **2008**, *621*, 314.
(22) Braunschweig, B.; Mukherjee, P.; Dlott, D. D.; Wieckowski, A. *J. Am. Chem. Soc.* **2010**, *132*, 14036.
(23) Bagchi, S.; Boxer, S. G.; Fayer, M. D. *J. Phys. Chem. B* **2012**, *116*, 4034.
(24) Fafarman, A. T.; Boxer, S. G. *J. Phys. Chem. B* **2010**, *114*, 13536.
(25) Fried, S. D.; Bagchi, S.; Boxer, S. G. *Science* **2014**, *346*, 1510.
(26) Fried, S. D.; Boxer, S. G. *Acc. Chem. Res.* **2015**, *48*, 998.
(27) Layfield, J. P.; Hammes-Schiffer, S. *J. Am. Chem. Soc.* **2013**, *135*, 717.
(28) Liu, C. T.; Layfield, J. P.; Stewart, R. J.; French, J. B.; Hanoian, P.; Asbury, J. B.; Hammes-Schiffer, S.; Benkovic, S. J. *J. Am. Chem. Soc.* **2014**, *136*, 10349.
(29) Nyquist, R. A. *Appl. Spectrosc.* **1990**, *44*, 1405.
(30) Onsager, L. *J. Am. Chem. Soc.* **1936**, *58*, 1486.
(31) Bagchi, S.; Fried, S. D.; Boxer, S. G. *J. Am. Chem. Soc.* **2012**, *134*, 10373.
(32) Fried, S. D.; Wang, L. P.; Boxer, S. G.; Ren, P.; Pande, V. S. *J. Phys. Chem. B* **2013**, *117*, 16236.
(33) Andrews, S. S.; Boxer, S. G. *J. Phys. Chem. A* **2000**, *104*, 11853.
(34) Raschke, M. B.; Shen, Y. R. *Encyclopedia of Modern Optics* **2004**, 184.
(35) Geiger, F. M. *Annu. Rev. Phys. Chem.* **2009**, *60*, 61.
(36) Baldelli, S. *Acc. Chem. Res.* **2008**, *41*, 421.

DOI: 10.1021/jacs.6b11940
J. Am. Chem. Soc. 2017, 139, 2369−2378

(37) Superfine, R.; Guyot-Sionnest, P.; Hunt, J.; Kao, C.; Shen, Y. *Surf. Sci.* **1988**, *200*, L445.
(38) Rivera-Rubero, S.; Baldelli, S. *J. Phys. Chem. B* **2004**, *108*, 15133.
(39) Yang, Y. Y.; Zhang, L. N.; Osawa, M.; Cai, W. B. *J. Phys. Chem. Lett.* **2013**, *4*, 1582.
(40) Deb, P.; Haldar, T.; Kashid, S. M.; Banerjee, S.; Chakrabarty, S.; Bagchi, S. *J. Phys. Chem. B* **2016**, *120*, 4034.
(41) Getahun, Z.; Huang, C. Y.; Wang, T.; De Leon, B.; DeGrado, W. F.; Gai, F. *J. Am. Chem. Soc.* **2003**, *125*, 405.
(42) Purcell, K. F.; Drago, R. S. *J. Am. Chem. Soc.* **1966**, *88*, 919.
(43) Wohlfahrth, C.; Wohlfarth, B. In *Optical Constants: Refractive Indices of Organic Liquids. SubVol. B*; Lechner, M. D., Ed.; Springer: Heidelberg, 1996.
(44) Li, H. H. *J. Phys. Chem. Ref. Data* **1980**, *9*, 161.
(45) Shalhout, F. Y.; Malyk, S.; Benderskii, A. V. *J. Phys. Chem. Lett.* **2012**, *3*, 3493.
(46) Beale, T. M.; Chudzinski, M. G.; Sarwar, M. G.; Taylor, M. S. *Chem. Soc. Rev.* **2013**, *42*, 1667.
(47) Politzer, P.; Murray, J. S.; Clark, T. *Phys. Chem. Chem. Phys.* **2013**, *15*, 11178.
(48) Varadwaj, P. R.; Varadwaj, A.; Jin, B.-Y. *Phys. Chem. Chem. Phys.* **2014**, *16*, 19573.
(49) Desiraju, G. R.; Harlow, R. L. *J. Am. Chem. Soc.* **1989**, *111*, 6757.
(50) Swords, W. B.; Simon, S. J. C.; Parlane, F. G. L.; Dean, R. K.; Kellett, C. W.; Hu, K.; Meyer, G. J.; Berlinguette, C. P. *Angew. Chem., Int. Ed.* **2016**, *55*, 5956.
(51) Levinson, N. M.; Fried, S. D.; Boxer, S. G. *J. Phys. Chem. B* **2012**, *116*, 10470.
(52) Fried, S. D.; Bagchi, S.; Boxer, S. G. *J. Am. Chem. Soc.* **2013**, *135*, 11181.
(53) Fafarman, A. T.; Sigala, P. A.; Herschlag, D.; Boxer, S. G. *J. Am. Chem. Soc.* **2010**, *132*, 12811.
(54) Green, J. H. S.; Harrison, D. J. *Spectrochim. Acta, Part A* **1976**, *32*, 1279.
(55) Borst, D. R.; Korter, T. M.; Pratt, D. W. *Chem. Phys. Lett.* **2001**, *350*, 485.
(56) Leffler, J. E.; Grunwald, E. *Rates and Equilibria of Organic Reactions as Treated by Statistical, Thermodynamic, and Extrathermodynamic Methods*; Dover Publications: New York, 1963.
(57) Le Fevre, R. J. W.; Orr, B. J.; Ritchie, G. L. D. *J. Chem. Soc.* **1965**, 2499.
(58) Frey, S.; Stadler, V.; Heister, K.; Eck, W.; Zharnikov, M.; Grunze, M.; Zeysing, B.; Terfort, A. *Langmuir* **2001**, *17*, 2408.
(59) Ballav, N.; Schüpbach, B.; Dethloff, O.; Feulner, P.; Terfort, A.; Zharnikov, M. *J. Am. Chem. Soc.* **2007**, *129*, 15416.

DOI: 10.1021/jacs.6b11940
J. Am. Chem. Soc. 2017, 139, 2369−2378